Mechanics of Advanced Materials and Structures, 13:357–369, 2006

ISSN: 1537-6494 print / 1537-6532 online
DOI: 10.1080/15376490600777665

Taylor & Francis
Taylor & Francis Group

On Higher-Order Modelling of Smart Beams with Embedded Shear-Mode Piezoceramic Actuators and Sensors

Marcelo A. Trindade
São Carlos School of Engineering, University of São Paulo, São Carlos, Brazil

Ayech Benjeddou
Institut Supérieur de Mécanique de Paris, Saint Ouen, France

A refined sandwich beam model is proposed in the present work. The mechanical model is a refinement of the classical sandwich theory (CST), where the core is modelled with a third-order shear deformation theory (TSDT). It is shown that the electromechanical coupling with the higher-order strains requires a third-order through-thickness model for the electric potential. Using these assumptions, a finite element (FE) model is developed considering, through the beam length, electrically: constant electric difference of potentials for the piezoelectric facing and core layers and quadratic third-order variable of the electric potential in the core, while mechanically: linear axial displacement and quadratic bending rotation of the core, and cubic transverse displacement of the sandwich beam. The proposed FE model is then compared with analytical and numerical CST, that use a first-order shear deformation theory (FSDT) in the core, and analytical equivalent single layer (ESL) models for a continuous piezoceramic core. It is shown that even when acting as an actuator, there exists a third-order induced potential in the piezoceramic material which may yield an overall stiffer structure. A comparison between FSDT and TSDT FE results for a piezoceramic embedded in an elastic core is also performed to evaluate the electrical and mechanical model refinements.

1. INTRODUCTION

Piezoelectric actuators have been widely used for the design of smart structures over the last two decades. They can be either surface-mounted or embedded into a host structure. Surface-mounted actuators are normally poled in the thickness direction, so that they act as extension actuators. However, this configuration subjects the actuators to high stresses and possible contact with foreign objects which are undesired for these brittle piezoceramics. These problems can be alleviated by using axially poled piezoceramic actuators sandwiched between two elastic layers, as proposed by Sun and Zhang [1]. In this case, the application of an electric field in the thickness direction induces transverse shear deformation of the actuator thus generating the desired transverse deflection of the sandwich structure.

After the pioneer works of Sun and Zhang [1, 2], several researchers have been interested in piezoelectric shear actuation. Through the use of a classical sandwich beam theory, Benjeddou et al. [3–5] showed that shear actuators induce distributed actuation moments in the structure unlike extension actuators which induce boundary forces. Therefore, the shear actuation mechanism may lead to fewer problems of debonding in actuators boundaries and to minor dependence of the control performance on actuators position and length. Aldraihem and Khdeir [6–8] presented exact solutions for sandwich beams with shear and extension actuators using equivalent single layer models based on first-order and third-order shear deformation theories. Trindade et al. [9] presented a comparison between active control performances of shear and extension actuation mechanisms using a sandwich beam finite element model. They showed that shear actuators are generally more suitable to control bending vibrations of stiff structures. Raja et al. [10] also studied active damping performance in composite materials using shear actuators as compared to that using the widespread extension actuators. Their results showed that shear actuators have promising features for vibration control applications, in particular the shear actuator was observed to be more effective in velocity feedback than the extension actuator. In a later work [11], Raja et al. have presented a finite element static analysis of sandwich beams actuated simultaneously by shear and extension actuators for several boundary conditions. Vel and Batra [12] presented an exact 3D solution for the static cylindrical bending of simply supported laminated plates with embedded shear piezoelectric actuators. Their analysis has shown that both longitudinal and shear stresses within the actuator are significantly smaller for the shear actuator. Recently, Edery-Azulay and Abramovich [13] presented closed-form solutions for the static analysis of

Received 15 March 2006; accepted 31 March 2006.
Address correspondence to M. A. Trindade, Department of Mechanical Engineering, São Carlos School of Engineering, University of São Paulo, Av. Trabalhador São-Carlense, 400, 13566-590 São Carlos-SP, Brazil. E-mail: trindade@sc.usp.br

laminate/sandwich beams with embedded extension and shear actuators. Achievements, trends and perspectives of the use of shear-mode piezoceramics in smart structures applications have recently been presented in [14, 15].

Although this so-called shear actuation mechanism seems quite promising for structural control, its modelling is still an open issue. Indeed, most of the existing refined models for piezoelectric laminate/sandwich structures focus on extension actuators, thus leading at most, to higher-order mechanical models but simple low order electrical models, since extension actuators present a simpler electrical behavior [16]. For shear actuated piezoelectric sandwich beams, either the classical sandwich theory (CST), with a first-order shear deformation (Timoshenko) for the core [2, 17], or first and higher-order equivalent single layer (ESL) theories [8, 18] were used. However, on one hand, it is very difficult to model the localized core shear deformation through ESL theories, and, on the other hand, the correct estimation of the core shear deformation is determinant to evaluate the sandwich beam induced deflection.

Hence, a refined sandwich beam model is proposed in the present work. The mechanical model is a refinement of CST, for which the facing layers respect Euler-Bernoulli assumptions and the core is modelled with the third-order shear deformation theory (TSDT) proposed by Reddy [19]. It is shown that the electromechanical coupling with the higher-order strains requires a third-order through-thickness model for the electric potential. Using these assumptions, a finite element (FE) model is developed considering, through the beam length, electrically: constant electric difference of potentials for the piezoelectric facing and core layers and quadratic third-order variable of the electric potential in the core, while mechanically: linear axial displacement and quadratic bending rotation of the core, and cubic transverse displacement of the sandwich beam. It is shown that, although more refined models are considered for the mechanical and electrical behaviors of the piezoelectric core, the resulting FE model has the same number of degrees of freedom (dof) as the previous CST one [17] due to a two-step static condensation of the internal dof of the bending rotation and third-order variable of the electric potential in the core. The proposed FE model is then compared with analytical and numerical CST [2, 17] and analytical ESL models [6] for a continuous piezoceramic core. Finally, a comparison between FSDT and TSDT FE models for a discontinuous elastic/piezoceramic core is performed to evaluate the effects of both electrical and mechanical refinements in the model.

2. THIRD-ORDER ELECTROMECHANICAL SANDWICH MODEL

A multilayer beam made of piezoelectric layers is modelled using a classical sandwich theory. Therefore, the beam is supposed to consist of a core layer sandwiched between top and bottom laminate face layers. The latter respect Euler-Bernoulli assumptions and hence are modelled using the classical laminate theory. On the contrary, the core is allowed to present shear strains, which are modelled using the TSDT proposed by Reddy [19]. For simplicity, all layers are assumed to be made of orthotropic piezoelectric materials, perfectly bonded and in plane stress state. In addition, the sub-layers of the faces are poled in the thickness direction while the core is poled in the longitudinal direction. However, both have electrodes covering completely their top and bottom skins. The length, width and thickness of the beam are denoted by L, b and h, respectively. Quantities relative to the upper, core and lower layers are represented by the subscripts a_j, c and b_j, where the subscript $j = \{1, \ldots, (n, m)\}$ denotes a sub-layer of the laminate faces. n and m are the number of sub-layers in the faces a and b respectively.

2.1. Displacements and Strains

From the assumptions cited previously, the axial and transverse displacement fields of faces and core may be written in the following general form (also see Figure 1)

$$\begin{aligned}
\breve{u}_k(x, y, z) &= u_k(x) + (z - z_k)\beta_k(x); \quad k = a, b \\
\breve{u}_c(x, y, z) &= u_c(x) + (z - z_c)\beta_c(x) - \frac{4(z - z_c)^3}{3h_c^2} \\
&\quad \times [\beta_c(x) + w(x)'] \\
\breve{w}_i(x, y, z) &= w(x); \quad i = a, b, c
\end{aligned} \tag{1}$$

Notice that the same displacement fields u_k ($k = a, b$) are considered for all sub-layers k_j of the face k. From Euler-Bernoulli hypotheses, $\beta_k = -w'$ ($k = a, b$), where, $\bullet'$ is used to denote $\partial \bullet / \partial x$. The mid-plan of the core is set to coincide with the origin of the z-axis, so that $z_c = 0$.

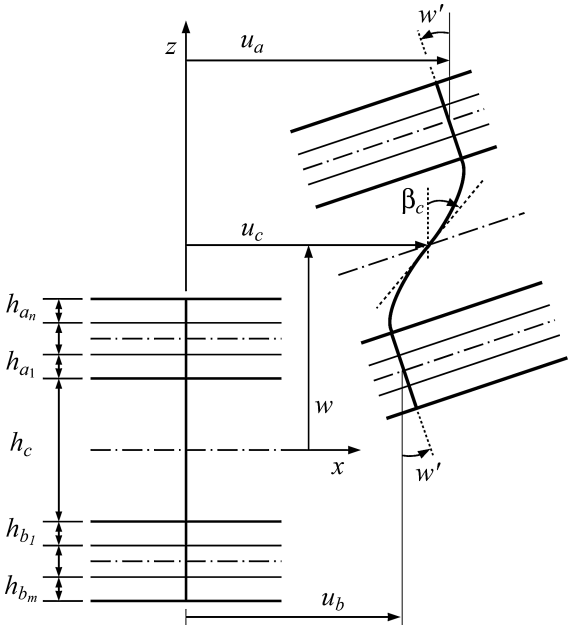

FIG. 1. Kinematics representation of the multilayer faces sandwich beam with third-order shear deformation theory for the core.

Using the displacement continuity conditions between layers, the displacement fields (1) may be written in terms of only three main variables. It is chosen then to write the displacements of the face layers neutral line, u_a and u_b, in terms of the axial displacement and section rotation of the core, u_c and β_c. Consequently, the i-th layer displacement fields may be rewritten in terms of the three model independent mechanical variables u_c, β_c and w as

$$\begin{aligned}
\breve{u}_k(x,z) &= \left(u_c \pm \frac{h_c\beta_c}{3} \mp d_k w'\right) - (z-z_k)w'; \\
&\qquad\qquad k = a(+), b(-) \\
\breve{u}_c(x,z) &= u_c + z\beta_c - \frac{4z^3}{3h_c^2}(\beta_c + w') \\
\breve{w}_i(x,z) &= w(x); \quad i = a,b,c
\end{aligned} \tag{2}$$

where

$$\begin{aligned}
d_k &= \frac{3h_k + h_c}{6}; \quad z_k = \pm\frac{h_k + h_c}{2}; \\
h_k &= \sum_{j=1}^{n,m} h_{k_j}; \quad k = a(+,n), b(-,m)
\end{aligned}$$

The usual strain-displacement relations for each layer yield the following axial ε_1 and shear ε_5 strains for the i-th layer

$$\begin{aligned}
\varepsilon_{1k} &= \varepsilon_k^m + (z-z_k)\varepsilon_k^b \\
\varepsilon_{1c} &= \varepsilon_c^m + z\varepsilon_c^b - \frac{4z^3}{3h_c^2}\varepsilon_c^h \\
\varepsilon_{5c} &= \left(1 - \frac{4z^2}{h_c^2}\right)\varepsilon_c^s
\end{aligned} \tag{3}$$

where

$$\begin{aligned}
&\varepsilon_k^m = u_c' \pm \frac{h_c\beta_c'}{3} \mp d_k w''; \quad \varepsilon_k^b = -w''; \quad k = a(+), b(-) \\
&\varepsilon_c^m = u_c'; \quad \varepsilon_c^b = \beta_c'; \quad \varepsilon_c^h = \beta_c' + w''; \quad \varepsilon_c^s = \beta_c + w'
\end{aligned}$$

Notice that the parameters d_k ($k = a, b$) are membrane-bending coupling parameters. Notice also that $\varepsilon_c^h = \varepsilon_c^b - \varepsilon_k^b = (\varepsilon_c^s)'$, meaning that the higher-order strain corresponds to a relative bending deformation between faces and core.

2.2. Reduced Piezoelectric Constitutive Equations

Linear orthotropic piezoelectric materials with material symmetry axes parallel to the beam ones are considered here. c_{ij}, e_{kj} and ϵ_{kk} ($i, j = 1, \ldots, 6; k = 1, 2, 3$) denote their elastic, piezoelectric and dielectric material constants.

The piezoelectric face sub-layers are poled transversely and subjected to transverse electrical fields only. Hence, the three-dimensional linear constitutive equations of the face sub-layer k_j can be reduced [3] to

$$\begin{Bmatrix} \sigma_{1k_j} \\ D_{3k_j} \end{Bmatrix} = \begin{bmatrix} c_{11}^{k_j *} & -e_{31}^{k_j *} \\ e_{31}^{k_j *} & \epsilon_{33}^{k_j *} \end{bmatrix} \begin{Bmatrix} \varepsilon_{1k} \\ E_{3k_j} \end{Bmatrix} \tag{4}$$

where,

$$\begin{aligned}
&c_{11}^{k_j *} = c_{11}^{k_j} - \frac{c_{13}^{k_j 2}}{c_{33}^{k_j}}; \quad e_{31}^{k_j *} = e_{31}^{k_j} - \frac{c_{13}^{k_j}}{c_{33}^{k_j}} e_{33}^{k_j}; \\
&\epsilon_{33}^{k_j *} = \epsilon_{33}^{k_j} + \frac{e_{33}^{k_j 2}}{c_{33}^{k_j}}
\end{aligned}$$

σ_{1k_j}, ε_{1k}, D_{3k_j} and E_{3k_j} are axial stress and strain, and transverse electrical displacement and field. The modification of the material constants is due to the plane stress assumption ($\sigma_3 = 0$).

The piezoelectric core layer is poled in the axial direction. Its constitutive equations can be obtained from those of the surface layers through a rotation, so that axial and transverse indices interchange. Therefore, the reduced constitutive equations of the piezoelectric core are

$$\begin{Bmatrix} \sigma_{1c} \\ \sigma_{5c} \\ D_{1c} \\ D_{3c} \end{Bmatrix} = \begin{bmatrix} c_{33}^{c*} & 0 & -e_{33}^{c*} & 0 \\ 0 & c_{55}^{c} & 0 & -e_{15}^{c} \\ e_{33}^{c*} & 0 & \epsilon_{33}^{c*} & 0 \\ 0 & e_{15}^{c} & 0 & \epsilon_{11}^{c} \end{bmatrix} \begin{Bmatrix} \varepsilon_{1c} \\ \varepsilon_{5c} \\ E_{1c} \\ E_{3c} \end{Bmatrix} \tag{5}$$

where

$$c_{33}^{c*} = c_{33}^{c} - \frac{c_{13}^{c\,2}}{c_{11}^{c}}; \quad e_{33}^{c*} = e_{33}^{c} - \frac{c_{13}^{c}}{c_{11}^{c}} e_{31}^{c}; \quad \epsilon_{33}^{c*} = \epsilon_{33}^{c} + \frac{e_{31}^{c\,2}}{c_{11}^{c}}$$

and σ_{5c}, ε_{5c}, D_{1c} and E_{1c} are transverse shear stress and strain, and axial electrical displacement and field. The material constants modification is also due to the plane stress assumption for the core ($\sigma_3 = 0$).

Notice the presence in Eq. (5) of both axial and transverse components of the electric field and displacement.

2.3. Electric Potentials and Fields

A constant transverse electrical field is assumed for the face piezoelectric sub-layers and the remaining in-plane components are supposed to vanish. Consequently it is, for the k_j-th face piezoelectric sub-layer,

$$E_{3k_j} = -\frac{V_{k_j}}{h_{k_j}} \tag{6}$$

where V_{k_j} is the difference of electric potential of the k_j-th laminae, defined by $V_{k_j} = V_{k_j}^+ - V_{k_j}^-$, with $V_{k_j}^+$ and $V_{k_j}^-$ being the voltages applied on the upper and lower skins of the k_j-th piezoelectric face sub-layer.

On the contrary, both axial and transverse electrical fields are considered for the core piezoelectric layer. In addition, the transverse one is assumed to be quadratic through thickness and not constant as for the face sub-layers. Hence, the electric potential in the core is assumed cubic through thickness and in the following form,

$$\Psi(x,z) = \Psi_0(x) + \frac{z}{h_c}\Psi_1(x) + \frac{z^2}{h_c^2}\Psi_2(x) + \frac{z^3}{h_c^3}\Psi_3(x) \tag{7}$$

It is worthwhile to rewrite the electric potential (7) in terms of the mean and difference of electric potential on the upper and lower skins of the piezoelectric core,

$$\Psi(x,h_c/2) = \Psi^+ \quad \text{and} \quad \Psi(x,-h_c/2) = \Psi^- \quad \rightsquigarrow$$
$$\Psi_1 + \frac{\Psi_3}{4} = V_c \quad \text{and} \quad \Psi_0 + \frac{\Psi_2}{4} = \Psi_m$$

where

$$V_c = \Psi^+ - \Psi^-; \quad \Psi_m = \frac{\Psi^+ + \Psi^-}{2} \tag{8}$$

Notice that for a piezoelectric patch with upper and bottom skins fully covered by electrodes, the electric potentials Ψ^+ and Ψ^-, and thus both V_c and Ψ_m, are constant in the axial direction. Hence, the electric potential (7) may be rewritten as

$$\Psi(x,z) = \Psi_m + \frac{z}{h_c}V_c + \left(\frac{z^2}{h_c^2} - \frac{1}{4}\right)\Psi_2(x) + \left(\frac{z^2}{h_c^2} - \frac{1}{4}\right)\frac{z}{h_c}\Psi_3(x) \tag{9}$$

The axial $E_{1c} = -\partial\Psi/\partial x$ and transverse $E_{3c} = -\partial\Psi/\partial z$ electrical fields may then be evaluated from the electric potential (9) leading to

$$\begin{aligned} E_{1c} &= -\left(\frac{z^2}{h_c^2} - \frac{1}{4}\right)\Psi_2' - \left(\frac{z^2}{h_c^2} - \frac{1}{4}\right)\frac{z}{h_c}\Psi_3' \\ E_{3c} &= -\frac{V_c}{h_c} - \frac{z}{h_c}\frac{2\Psi_2}{h_c} - \left(\frac{3z^2}{h_c^2} - \frac{1}{4}\right)\frac{\Psi_3}{h_c} \end{aligned} \tag{10}$$

Notice that the axial electric field is only due to the electric potential higher-order terms. Moreover, it vanishes on the upper and lower surfaces of the piezoceramic core (see Eq. (10)). The choice of a cubic electric potential is justified by the solution of the electrostatic equilibrium equation

$$D_{1c,1} + D_{2c,2} + D_{3c,3} = 0 \tag{11}$$

Noting that $D_{2c,2}$ is assumed to vanish and replacing D_{1c} and D_{3c}, of the core constitutive Eqs. (5), in the last equation lead to

$$e_{33}^{c*}\frac{\partial\varepsilon_{1c}}{\partial x} + \epsilon_{33}^{c*}\frac{\partial E_{1c}}{\partial x} + e_{15}^{c}\frac{\partial\varepsilon_{5c}}{\partial z} + \epsilon_{11}^{c}\frac{\partial E_{3c}}{\partial z} = 0 \tag{12}$$

Using the definitions of axial and shear strains (3), in terms of the generalized membrane, bending, higher-order and shear strains, and the electric field-potential relations together with Eq. (7), the last equation may be rewritten leading to the relations

$$\begin{aligned} \epsilon_{33}^{c*}\frac{1}{4}\Psi_2'' - \epsilon_{11}^{c}\frac{2}{h_c}\frac{\Psi_2}{h_c} + e_{33}^{c*}\varepsilon_c^{m\prime} &= 0 \\ \epsilon_{33}^{c*}\frac{1}{4}\frac{\Psi_3''}{h_c} - \epsilon_{11}^{c}\frac{6}{h_c^2}\frac{\Psi_3}{h_c} + e_{33}^{c*}\varepsilon_c^{b\prime} - e_{15}^{c}\frac{8}{h_c^2}\varepsilon_c^{s} &= 0 \\ \epsilon_{33}^{c*}\frac{\Psi_2''}{h_c^2} &= 0 \\ \epsilon_{33}^{c*}\frac{\Psi_3''}{h_c^3} + e_{33}^{c*}\frac{4}{3h_c^2}\varepsilon_c^{h\prime} &= 0 \end{aligned} \tag{13}$$

or, alternatively, writing these conditions in terms of the main variables, u_c, β_c and w, yields

$$\begin{aligned} \epsilon_{33}^{c*}\frac{1}{4}\Psi_2'' - \epsilon_{11}^{c}\frac{2}{h_c}\frac{\Psi_2}{h_c} + e_{33}^{c*}u_c'' &= 0 \\ \epsilon_{33}^{c*}\frac{1}{4}\frac{\Psi_3''}{h_c} - \epsilon_{11}^{c}\frac{6}{h_c^2}\frac{\Psi_3}{h_c} + e_{33}^{c*}\beta_c'' - e_{15}^{c}\frac{8}{h_c^2}(\beta_c + w') &= 0 \\ \epsilon_{33}^{c*}\frac{\Psi_2''}{h_c^2} &= 0 \\ \epsilon_{33}^{c*}\frac{\Psi_3''}{h_c^3} + e_{33}^{c*}\frac{4}{3h_c^2}(\beta_c'' + w''') &= 0 \end{aligned} \tag{14}$$

Conditions (13) show that Ψ_2 is only coupled to the axial strain of the core, while Ψ_3 is coupled to bending, shear and higher-order strains. If a linear approximation for u_c is considered, (14) yields $\Psi_2 = 0$. On the other hand, as long as there is shear strain in the core, a cubic electric potential is induced through Ψ_3, as shown in (13). Also, in case of a cubic approximation for w, conditions (14) require a quadratic approximation for β_c and Ψ_3. This justifies the choice of a cubic through-thickness electric potential. Although conditions (14) allow the evaluation of the electric potential in the core from the mechanical variables u_c, β_c and w, let us assume for now that it is arbitrary as in (9) but with $\Psi_2 = 0$. This leads to the following electric potential

$$\Psi(x,z) = \Psi_m + \frac{z}{h_c}V_c + \left(\frac{z^2}{h_c^2} - \frac{1}{4}\right)\frac{z}{h_c}\Psi_3(x) \tag{15}$$

and hence to the following axial and transverse electrical fields (as in (10) but with $\Psi_2 = 0$)

$$E_{1c} = -\left(\frac{z^2}{h_c^2} - \frac{1}{4}\right)\frac{z}{h_c}\Psi_3', \quad E_{3c} = -\frac{V_c}{h_c} - \left(\frac{3z^2}{h_c^2} - \frac{1}{4}\right)\frac{\Psi_3}{h_c} \tag{16}$$

From Eqs. (6) and (16), it is clear that the electric model independent variables are V_{k_j}, V_c and Ψ_3.

2.4. Piezoelectric Variational Formulation

A variational formulation may be written using the virtual work principle extended to the piezoelectric media

$$\delta W - \delta H = 0; \quad \forall \delta u_c, \delta\beta_c, \delta w, \delta V_{k_j}, \delta V_c, \delta\Psi_3 \tag{17}$$

where δH and δW are the virtual works of electromechanical internal and applied mechanical forces, respectively.

The virtual work done by the electromechanical internal forces in the layered piezoelectric faces sandwich beam is

$$\delta H = \delta H_c + \sum_{k=a}^{b}\sum_{j=1}^{n,m} \delta H_{k_j} \tag{18}$$

where,

$$\delta H_{k_j} = \int_{\Omega_{k_j}} (\sigma_{1k_j}\delta\varepsilon_{1k} - D_{3k_j}\delta E_{3k_j})\mathrm{d}\Omega_{k_j}$$

$$\delta H_c = \int_{\Omega_c} (\sigma_{1c}\delta\varepsilon_{1c} + \sigma_{5c}\delta\varepsilon_{5c} - D_{1c}\delta E_{1c} - D_{3c}\delta E_{3c})\mathrm{d}\Omega_c$$

Ω_{k_j} and Ω_c are the volume of the k_j-th sub-layer and the core, respectively.

Using strain definitions (3), constitutive Eqs. (4) and (5), and electrical field relations (6) and (16), then integrating through thickness, the above equations for the k_j-th face sub-layer and core become

$$\begin{aligned}\delta H_{k_j} = \int_0^L \Big[& c_{11}^{k_j *}\big(A_{k_j}\delta\varepsilon_k^m\varepsilon_k^m + \bar{I}_{k_j}\delta\varepsilon_k^m\varepsilon_k^b + \bar{I}_{k_j}\delta\varepsilon_k^b\varepsilon_k^m \\ & + I_{k_j}\delta\varepsilon_k^b\varepsilon_k^b\big) + e_{31}^{k_j *}\big(A_{k_j}\delta\varepsilon_k^m + \bar{I}_{k_j}\delta\varepsilon_k^b\big)\frac{V_{k_j}}{h_{k_j}} \\ & + e_{31}^{k_j *}\frac{\delta V_{k_j}}{h_{k_j}}\big(A_{k_j}\varepsilon_k^m + \bar{I}_{k_j}\varepsilon_k^b\big) - \epsilon_{33}^{k_j *}A_{k_j}\frac{\delta V_{k_j}}{h_{k_j}}\frac{V_{k_j}}{h_{k_j}}\Big]\mathrm{d}x\end{aligned} \tag{19}$$

$$\begin{aligned}\delta H_c = \int_0^L \Big\{ & \delta\varepsilon_c^m c_{33}^{c*}A_c\varepsilon_c^m \\ & + \delta\varepsilon_c^b\left[c_{33}^{c*}I_c\left(\varepsilon_c^b - \frac{1}{5}\varepsilon_c^h\right) - e_{33}^{c*}\frac{2\bar{I}_c}{3}\frac{\Psi_3'}{h_c^3}\right] \\ & + \delta\varepsilon_c^h\left[c_{33}^{c*}I_c\left(-\frac{1}{5}\varepsilon_c^b + \frac{1}{21}\varepsilon_c^h\right) + e_{33}^{c*}\frac{2\bar{I}_c}{21}\frac{\Psi_3'}{h_c^3}\right] \\ & + \delta\varepsilon_c^s\left[\frac{8}{15}c_{55}^c A_c\varepsilon_c^s + e_{15}^c\left(\frac{2A_c}{3}\frac{V_c}{h_c} - \frac{4I_c}{5}\frac{\Psi_3}{h_c^3}\right)\right] \\ & + \frac{\delta V_c}{h_c}\left[e_{15}^c\frac{2A_c}{3}\varepsilon_c^s - \epsilon_{11}^c A_c\frac{V_c}{h_c}\right] \\ & + \frac{\delta\Psi_3'}{h_c^3}\left[e_{33}^{c*}\left(-\frac{2\bar{I}_c}{3}\varepsilon_c^b + \frac{2\bar{I}_c}{21}\varepsilon_c^h\right) - \epsilon_{33}^{c*}\frac{8\bar{\bar{I}}_c}{15}\frac{\Psi_3'}{h_c^3}\right] \\ & - \frac{\delta\Psi_3}{h_c^3}\left[e_{15}^c\frac{4I_c}{5}\varepsilon_c^s + 4\epsilon_{11}^c\bar{I}_c\frac{\Psi_3}{h_c^3}\right]\Big\}\mathrm{d}x\end{aligned} \tag{20}$$

A_{k_j}, $\bar{I}_{k_j}$ and I_{k_j} are, respectively, the area and the first and second moments of area of the k_j-th face sub-layer cross section, defined as

$$[A_{k_j}, \bar{I}_{k_j}, I_{k_j}] = \int_{-b/2}^{b/2}\int_{z_{k_j}-h_{k_j}/2}^{z_{k_j}+h_{k_j}/2} [1, (z-z_k), (z-z_k)^2]\mathrm{d}z\,\mathrm{d}y \tag{21}$$

where the local z-axis of the k_j-th sub-layer is situated at

$$z_{k_j} = \pm\frac{h_{k_j}+h_c}{2} \pm \sum_{r=1}^{j-1} h_{k_r}; \quad k = a(+), b(-) \tag{22}$$

For the core, A_c, I_c, $\bar{I}_c$ and $\bar{\bar{I}}_c$ are, respectively, the area and the second, fourth and sixth moments of area of its cross section, defined as

$$\left[A_c,\ I_c,\ \bar{I}_c,\ \bar{\bar{I}}_c\right] = \int_{-b/2}^{b/2}\int_{-h_c/2}^{h_c/2} [1,\ z^2,\ z^4,\ z^6]\,\mathrm{d}z\,\mathrm{d}y \tag{23}$$

One may notice from (20) that V_c is coupled to the core shear strain only. This term may be interpreted as the virtual work done by shearing moments $2A_c e_{15}^c V_c/3h_c$ induced by the applied voltage V_c. Its dual is the generalized shear strain ε_c^s, which is also the shear angle of the core. That is, only shear strain is induced by an axially constant applied difference of electric potential. Notice, however, that although the difference of potential V_c is constant in axial direction, the induced electrical field is not, due to the contribution of the variable Ψ_3.

The beam is subjected to surface axial and transversal forces at the boundaries of each face sub-layer ($F_x^{k_j}$,$F_z^{k_j}$) and core (F_x^c,F_z^c), and to body ones ($f_x^{k_j}$,$f_z^{k_j}$,f_x^c,f_z^c). Their virtual work on the beam can be written as

$$\delta W = \sum_{i=a}^{c} \delta W_i \tag{24}$$

where

$$\begin{aligned}\delta W_k = \sum_{j=1}^{n,m}\Big\{ & \Big[\int_{A_{k_j}} \big(F_x^{k_j}\delta\breve{u}_k + F_z^{k_j}\delta w\big)\mathrm{d}A_{k_j}\Big]_0^L \\ & + \int_{\Omega_{k_j}} \big(f_x^{k_j}\delta\breve{u}_k + f_z^{k_j}\delta w\big)\mathrm{d}\Omega_{k_j}\Big\}\end{aligned}$$

$$\begin{aligned}\delta W_c = & \Big[\int_{A_c} \big(F_x^c\delta\breve{u}_c + F_z^c\delta w\big)\mathrm{d}A_c\Big]_0^L \\ & + \int_{\Omega_c} \big(f_x^c\delta\breve{u}_c + f_z^c\delta w\big)\mathrm{d}\Omega_c\end{aligned}$$

Using displacement expressions (2), one may write the previous equations for the k-th face and the core, as

$$\delta W_k = \left[N_k \delta u_c \pm \frac{N_k h_c}{3} \delta\beta_c - (M_k \pm N_k d_k)\delta w' + Q_k \delta w \right]_0^L + \int_0^L \left(n_k \delta u_c \pm \frac{n_k h_c}{3} \delta\beta_c - (m_k \pm n_k d_k)\delta w' + q_k \delta w \right) \mathrm{d}x; \quad k = a(+), b(-) \tag{25}$$

$$\delta W_c = [\delta u_c N_c + \delta\beta_c M_c - \delta w' P_c + \delta w Q_c]_0^L + \int_0^L (\delta u_c n_c + \delta\beta_c m_c - \delta w' p_c + \delta w q_c)\mathrm{d}x \tag{26}$$

where the, boundary and distributed, normal, moment and shear resultants are defined as

$$\begin{aligned} N_k &= \sum_j N_{k_j}; \quad M_k = \sum_j M_{k_j}; \quad Q_k = \sum_j Q_{k_j} \\ n_k &= \sum_j n_{k_j}; \quad m_k = \sum_j m_{k_j}; \quad q_k = \sum_j q_{k_j} \end{aligned} \tag{27}$$

with

$$\begin{aligned} N_{k_j} &= \int F_x^{k_j} \mathrm{d}A_{k_j}; \quad M_{k_j} = \int F_x^{k_j}(z - z_k)\mathrm{d}A_{k_j} \\ Q_{k_j} &= \int F_z^{k_j} \mathrm{d}A_{k_j} \\ n_{k_j} &= \int f_x^{k_j} \mathrm{d}A_{k_j}; \quad m_{k_j} = \int f_x^{k_j}(z - z_k)\mathrm{d}A_{k_j} \\ q_{k_j} &= \int f_z^{k_j} \mathrm{d}A_{k_j} \\ N_c &= \int F_x^c \mathrm{d}A_c; \quad M_c = \int F_x^c \left(z - \frac{4z^3}{3h_c^2} \right) \mathrm{d}A_c \\ P_c &= \int F_x^c \frac{4z^3}{3h_c^2} \mathrm{d}A_c; \quad Q_c = \int F_z^c \mathrm{d}A_c \\ n_c &= \int f_x^c \mathrm{d}A_c; \quad m_c = \int f_x^c \left(z - \frac{4z^3}{3h_c^2} \right) \mathrm{d}A_c \\ p_c &= \int f_x^c \frac{4z^3}{3h_c^2} \mathrm{d}A_c; \quad q_c = \int f_z^c \mathrm{d}A_c \end{aligned}$$

Notice that a difference between the axial forces $F_x^{k_j}$ and $f_x^{k_j}$ ($j = 1, \ldots, (n, m)$) on each sub-layer of face k may induce bending moments M_k and m_k, due to the membrane-bending coupling caused by the first moment of area $\bar{I}_{k_j}$. Notice also that when the axial forces F_x^c and f_x^c applied in the core are asymmetric through thickness, they induce bending moments M_c and m_c and shear moments P_c and p_c. The latter are due to the higher-order terms considered in the displacement fields.

3. THIRD-ORDER PIEZOELECTRIC FINITE ELEMENT MODEL

Using the expressions of virtual works in the variational formulation, a finite element model for the piezoelectric sandwich/multilayer beam is developed. Lagrange linear shape functions are assumed for the axial displacement of the core, u_c. The electrical difference of potentials V_{k_j} of the l and p piezoelectric sub-layers of the faces a and b, respectively, and V_c of the piezoelectric core, are considered to be constant in the element. A quadratic shape function is assumed for the section rotation of the core β_c, to avoid shear locking, and for the third-order coefficient Ψ_3 in the core electric potential, to respect the electrostatic equilibrium conditions (13). For the transverse deflection w, Hermite cubic shape functions are assumed. Hence, the elementary degrees of freedom (dof) column vector $\hat{\mathbf{q}}$ is defined as

$$\hat{\mathbf{q}} = \mathrm{col}\Big(u_c^{(1)}, w^{(1)}, w'^{(1)}, \beta_c^{(1)}, \Psi_3^{(1)}, u_c^{(2)}, w^{(2)}, w'^{(2)}, \beta_c^{(2)}, \Psi_3^{(2)}, \beta_c^{(0)}, V_{a_1}^{(0)}, \ldots, V_{a_l}^{(0)}, V_{b_1}^{(0)}, \ldots, V_{b_p}^{(0)}, V_c^{(0)}, \Psi_3^{(0)} \Big) \tag{28}$$

where the $\hat{}$ will be used to define elementary quantities. Using this definition in the relations (19) and (20), the discretized virtual works of the elementary electromechanical internal forces of the face sub-layers $\delta\hat{H}_{k_j}$ and the core $\delta\hat{H}_c$ are

$$\begin{aligned} \delta\hat{H}_{k_j} &= \delta\hat{\mathbf{q}}^{\mathrm{t}} \left(\hat{\mathbf{K}}_{k_j m} - \hat{\mathbf{K}}_{k_j me} - \hat{\mathbf{K}}_{k_j me}^{\mathrm{t}} + \hat{\mathbf{K}}_{k_j e} \right) \hat{\mathbf{q}} = \delta\hat{\mathbf{q}}^{\mathrm{t}} \hat{\mathbf{K}}_{k_j} \hat{\mathbf{q}} \\ \delta\hat{H}_c &= \delta\hat{\mathbf{q}}^{\mathrm{t}} \left(\hat{\mathbf{K}}_{cm} - \hat{\mathbf{K}}_{cme} - \hat{\mathbf{K}}_{cme}^{\mathrm{t}} + \hat{\mathbf{K}}_{ce} \right) \hat{\mathbf{q}} = \delta\hat{\mathbf{q}}^{\mathrm{t}} \hat{\mathbf{K}}_c \hat{\mathbf{q}} \end{aligned} \tag{29}$$

where the elementary mechanical $\hat{\mathbf{K}}_{k_j m}$, piezoelectric $\hat{\mathbf{K}}_{k_j me}$ and dielectric $\hat{\mathbf{K}}_{k_j e}$ stiffness matrices of k_j-th sub-layer of the faces are

$$\begin{aligned} \hat{\mathbf{K}}_{k_j m} &= \int_0^{L_e} c_{11}^{k_j *} \left[A_{k_j} \mathbf{B}_{km}^{\mathrm{t}} \mathbf{B}_{km} + \bar{I}_{k_j} \left(\mathbf{B}_{km}^{\mathrm{t}} \mathbf{B}_{kb} + \mathbf{B}_{kb}^{\mathrm{t}} \mathbf{B}_{km} \right) + I_{k_j} \mathbf{B}_{kb}^{\mathrm{t}} \mathbf{B}_{kb} \right] \mathrm{d}x \\ \hat{\mathbf{K}}_{k_j me} &= -\int_0^{L_e} e_{31}^{k_j *} \frac{1}{h_{k_j}} \left(A_{k_j} \mathbf{B}_{km}^{\mathrm{t}} + \bar{I}_{k_j} \mathbf{B}_{kb}^{\mathrm{t}} \right) \mathbf{N}_{pkj} \mathrm{d}x \\ \hat{\mathbf{K}}_{k_j e} &= -\int_0^{L_e} \epsilon_{33}^{k_j *} \frac{A_{k_j}}{h_{k_j}^2} \mathbf{N}_{pkj}^{\mathrm{t}} \mathbf{N}_{pkj} \mathrm{d}x \end{aligned} \tag{30}$$

L_e is the element length. $\mathbf{B}_{km}$ and $\mathbf{B}_{kb}$ are the membrane (m) and bending (b) strain operators of the faces. $\mathbf{N}_{pkj}$ is the interpolation matrix used for the difference of electric potential V_{k_j} in the faces sub-layers.

The elementary stiffness matrices of the core $\hat{\mathbf{K}}_{cm}$, $\hat{\mathbf{K}}_{cme}$ and $\hat{\mathbf{K}}_{ce}$ are written as

$$\begin{aligned}
\hat{\mathbf{K}}_{cm} &= \int_0^{L_e} \left\{ c_{33}^{c*} \Big[A_c \mathbf{B}_{cm}^{\mathrm{t}} \mathbf{B}_{cm} + I_c \mathbf{B}_{cb}^{\mathrm{t}} \mathbf{B}_{cb} \right. \\
&\quad - \frac{I_c}{5} \left(\mathbf{B}_{cb}^{\mathrm{t}} \mathbf{B}_{ch} + \mathbf{B}_{ch}^{\mathrm{t}} \mathbf{B}_{cb} \right) + \frac{I_c}{21} \mathbf{B}_{ch}^{\mathrm{t}} \mathbf{B}_{ch} \Big] \\
&\quad \left. + \frac{8}{15} c_{55}^{c} A_c \mathbf{B}_{cs}^{\mathrm{t}} \mathbf{B}_{cs} \right\} \mathrm{d}x \\
\hat{\mathbf{K}}_{cme} &= -\int_0^{L_e} \left\{ e_{33}^{c*} \left(-\frac{2\bar{I}_c}{3h_c^3} \mathbf{B}_{cb}^{\mathrm{t}} \mathbf{N}'_{\Psi 3} + \frac{2\bar{I}_c}{21h_c^3} \mathbf{B}_{ch}^{\mathrm{t}} \mathbf{N}'_{\Psi 3} \right) \right. \\
&\quad \left. + e_{15}^{c} \mathbf{B}_{cs}^{\mathrm{t}} \left(\frac{2A_c}{3h_c} \mathbf{N}_{Vc} - \frac{4I_c}{5h_c^3} \mathbf{N}_{\Psi 3} \right) \right\} \mathrm{d}x \\
\hat{\mathbf{K}}_{ce} &= -\int_0^{L_e} \left\{ \epsilon_{33}^{c*} \frac{8\bar{\bar{I}}_c}{15h_c^6} \mathbf{N}'_{\Psi 3}{}^{\mathrm{t}} \mathbf{N}'_{\Psi 3} \right. \\
&\quad \left. + \epsilon_{11}^{c} \left(\frac{A_c}{h_c^2} \mathbf{N}_{Vc}^{\mathrm{t}} \mathbf{N}_{Vc} + \frac{4\bar{I}_c}{h_c^6} \mathbf{N}_{\Psi 3}^{\mathrm{t}} \mathbf{N}_{\Psi 3} \right) \right\} \mathrm{d}x \qquad (31)
\end{aligned}$$

where $\mathbf{B}_{cm}$, $\mathbf{B}_{cb}$, $\mathbf{B}_{ch}$ and $\mathbf{B}_{cs}$ are the membrane (m), bending (b), higher-order (h) and shear (s) strain operators. Notice that bending and higher-order strains of the core are coupled. The piezoelectric stiffness is composed of terms coupling shear strains with the electric variables V_c and Ψ_3 and terms coupling the derivative Ψ_3' with bending and higher-order strains. The latter are due to the axial component of the electrical field. The electric variables V_c and Ψ_3 are interpolated by the operators $\mathbf{N}_{Vc}$ and $\mathbf{N}_{\Psi 3}$.

The elementary virtual work of distributed applied mechanical forces may be written as

$$\delta \hat{W} = \delta \hat{\mathbf{q}}^T \hat{\mathbf{F}}_m \qquad (32)$$

where $\hat{\mathbf{F}}_m$ defines the vector of generalized distributed mechanical nodal forces obtained from (25) and (26),

$$\begin{aligned}
\hat{\mathbf{F}}_m = \int_0^{L_e} & \left[\mathbf{N}_{ax}^{\mathrm{t}} n_a + \mathbf{N}_{bx}^{\mathrm{t}} n_b + \mathbf{N}_{cx}^{\mathrm{t}} n_c + \mathbf{N}_{az}^{\mathrm{t}} (q_a + q_b + q_c) \right. \\
& \left. - \mathbf{N}_{ar}^{\mathrm{t}} (m_a + m_b) + \mathbf{N}_{cr}^{\mathrm{t}} m_c - \mathbf{N}_{cs}^{\mathrm{t}} p_c \right] \mathrm{d}x \qquad (33)
\end{aligned}$$

$\mathbf{N}_{ix}$, $\mathbf{N}_z$, $\mathbf{N}_{ir}$ and $\mathbf{N}_{cs}$ are the translation in x and z directions, rotation and shear interpolation matrices. The point forces contributions in (25) and (26) can be added *a posteriori* to the matricial system.

Using discretized expressions, one may obtain the elementary electromechanical internal forces virtual work of the sandwich/multilayer beam. Then, substituting the expressions of elementary discretized virtual works in (17), the discretized variational formulation for an element is written as

$$(\hat{\mathbf{K}}_f + \hat{\mathbf{K}}_c)\hat{\mathbf{q}} = \hat{\mathbf{F}}_m \qquad (34)$$

where $\hat{\mathbf{K}}_f = \sum_k \sum_j \hat{\mathbf{K}}_{kj}$. Notice that electric dofs may be eliminated from the dofs vector through a static condensation. Since there are elemental ($V_{a_j}^{(0)}$, $V_{b_j}^{(0)}$, $V_c^{(0)}$ and $\Psi_3^{(0)}$) and nodal ($\Psi_3^{(1)}$ and $\Psi_3^{(2)}$) electric dofs, the static condensation will be obtained in two steps. First, the unknown elemental electric dofs are condensed at the element level; then, after assembling, the nodal electric dofs are condensed at the global level. Notice that the static condensation at the element level may also be used to eliminate the internal mechanical dof $\beta_c^{(0)}$.

Therefore, let us decompose the electric dofs in prescribed elemental ones $\hat{\mathbf{q}}_a$, corresponding to the difference of potentials ($V_{a_j}^{(0)}$, $V_{b_j}^{(0)}$, $V_c^{(0)}$) applied to an actuator; unknown elemental ones $\hat{\mathbf{q}}_s$, corresponding to the difference of potentials ($V_{a_j}^{(0)}$, $V_{b_j}^{(0)}$, $V_c^{(0)}$) induced in a sensor and the unknown $\Psi_3^{(0)}$ for the piezoelectric core; and nodal ones $\hat{\mathbf{q}}_e$, corresponding to the unknown $\Psi_3^{(1)}$ and $\Psi_3^{(2)}$ for the core. Notice that even for an actuator in the core, for which $V_c^{(0)}$ is known and prescribed, the third-order variable Ψ_3 is unknown, that is $\Psi_3^{(1)}$, $\Psi_3^{(2)}$ and $\Psi_3^{(0)}$, since the applied difference of potential only determines Ψ^+ and Ψ^-, that is V_c. The mechanical dofs vector is also decomposed into the nodal $\hat{\mathbf{q}}_m$ and elemental $\hat{\mathbf{q}}_{mc}$ ones.

For the sake of clarity, the mechanical $\hat{\mathbf{q}}_{mc}$ and electrical $\hat{\mathbf{q}}_s$ elemental dofs to be condensed are assembled to form the vector $\hat{\mathbf{q}}_c = \mathrm{col}\,(\hat{\mathbf{q}}_{mc}, \hat{\mathbf{q}}_s)$ of dofs to be condensed at the element level. Then, the elementary dofs vector $\hat{\mathbf{q}}$ in (28) may be rewritten as $\hat{\mathbf{q}} = \mathrm{col}(\hat{\mathbf{q}}_m, \hat{\mathbf{q}}_e, \hat{\mathbf{q}}_c, \hat{\mathbf{q}}_a)$. Consequently, Eq. (34) may be decomposed in the following form

$$\begin{bmatrix} \hat{\mathbf{K}}_m & -\hat{\mathbf{K}}_{me} & -\hat{\mathbf{K}}_{mc} & -\hat{\mathbf{K}}_{ma} \\ & \hat{\mathbf{K}}_{ee} & \hat{\mathbf{K}}_{ec} & \hat{\mathbf{K}}_{ea} \\ & & \hat{\mathbf{K}}_{cc} & \hat{\mathbf{K}}_{ca} \\ & sym & & \hat{\mathbf{K}}_{aa} \end{bmatrix} \begin{Bmatrix} \hat{\mathbf{q}}_m \\ \hat{\mathbf{q}}_e \\ \hat{\mathbf{q}}_c \\ \hat{\mathbf{q}}_a \end{Bmatrix} = \begin{Bmatrix} \hat{\mathbf{F}}_m \\ \mathbf{0} \\ \hat{\mathbf{F}}_c \\ \mathbf{0} \end{Bmatrix} \qquad (35)$$

The differences of potential applied to the actuators $\hat{\mathbf{q}}_a$ are prescribed, hence their virtual variations $\delta\hat{\mathbf{q}}_a$ vanish. Therefore, the fourth line of Eq. (35) is automatically satisfied and may be ignored. In addition, the terms in the remaining lines, corresponding to $\hat{\mathbf{q}}_a$, can be moved to the right hand side leading, respectively, to the following equivalent electric load vectors

$$\hat{\mathbf{F}}_{ma} = \hat{\mathbf{K}}_{ma}\hat{\mathbf{q}}_a, \quad \hat{\mathbf{F}}_{ea} = -\hat{\mathbf{K}}_{ea}\hat{\mathbf{q}}_a, \quad \hat{\mathbf{F}}_{ca} = -\hat{\mathbf{K}}_{ca}\hat{\mathbf{q}}_a \qquad (36)$$

Since the stiffness matrix $\hat{\mathbf{K}}_{cc}$ corresponding to the unknown elemental dofs is non-singular, the third line of (35) can be solved for $\hat{\mathbf{q}}_c$ in terms of $\hat{\mathbf{q}}_m$ and $\hat{\mathbf{q}}_e$, leading to

$$\hat{\mathbf{q}}_c = \hat{\mathbf{K}}_{cc}^{-1} \left(\hat{\mathbf{F}}_c + \hat{\mathbf{F}}_{ca} + \hat{\mathbf{K}}_{mc}^{\mathrm{t}} \hat{\mathbf{q}}_m - \hat{\mathbf{K}}_{ec}^{\mathrm{t}} \hat{\mathbf{q}}_e \right) \qquad (37)$$

Equation (35) may then be statically condensed by replacing expressions (36) and (37) in the first and second lines and

eliminating the solved third and fourth lines,

$$\begin{bmatrix} \hat{\mathbf{K}}_m^* & -\hat{\mathbf{K}}_{me}^* \\ -\hat{\mathbf{K}}_{me}^{*\mathrm{t}} & \hat{\mathbf{K}}_{ee}^* \end{bmatrix} \begin{Bmatrix} \hat{\mathbf{q}}_m \\ \hat{\mathbf{q}}_e \end{Bmatrix} = \begin{Bmatrix} \hat{\mathbf{F}}_m + \hat{\mathbf{F}}_{ma}^* + \hat{\mathbf{F}}_{mc} \\ \hat{\mathbf{F}}_{ea}^* - \hat{\mathbf{F}}_{ec} \end{Bmatrix} \tag{38}$$

where the modified stiffness matrices are

$$\begin{aligned} \hat{\mathbf{K}}_m^* &= \hat{\mathbf{K}}_m - \hat{\mathbf{K}}_{mc}\hat{\mathbf{K}}_{cc}^{-1}\hat{\mathbf{K}}_{mc}^{\mathrm{t}} \quad \hat{\mathbf{K}}_{me}^* = \hat{\mathbf{K}}_{me} - \hat{\mathbf{K}}_{mc}\hat{\mathbf{K}}_{cc}^{-1}\hat{\mathbf{K}}_{ec}^{\mathrm{t}} \\ \hat{\mathbf{K}}_{ee}^* &= \hat{\mathbf{K}}_{ee} - \hat{\mathbf{K}}_{ec}\hat{\mathbf{K}}_{cc}^{-1}\hat{\mathbf{K}}_{ec}^{\mathrm{t}} \end{aligned} \tag{39}$$

and the generalized forces in the right-hand side are

$$\begin{aligned} \hat{\mathbf{F}}_{ma}^* &= \hat{\mathbf{F}}_{ma} + \hat{\mathbf{K}}_{mc}\hat{\mathbf{K}}_{cc}^{-1}\hat{\mathbf{F}}_{ca} \quad \hat{\mathbf{F}}_{mc} = \hat{\mathbf{K}}_{mc}\hat{\mathbf{K}}_{cc}^{-1}\hat{\mathbf{F}}_c \\ \hat{\mathbf{F}}_{ea}^* &= \hat{\mathbf{F}}_{ea} - \hat{\mathbf{K}}_{ec}\hat{\mathbf{K}}_{cc}^{-1}\hat{\mathbf{F}}_{ca} \quad \hat{\mathbf{F}}_{ec} = \hat{\mathbf{K}}_{ec}\hat{\mathbf{K}}_{cc}^{-1}\hat{\mathbf{F}}_c \end{aligned} \tag{40}$$

This equation allows to solve for the nodal mechanical $\hat{\mathbf{q}}_m$ and electrical $\hat{\mathbf{q}}_e$ dofs, when the beam is subjected to mechanical forces col($\hat{\mathbf{F}}_m$, $\hat{\mathbf{F}}_c$) and/or differences of electric potentials $\hat{\mathbf{q}}_a$, through the equivalent loads $\hat{\mathbf{F}}_{ma}$ and $\hat{\mathbf{F}}_{ea}$. The unknown elemental mechanical $\hat{\mathbf{q}}_{mc}$ and electrical $\hat{\mathbf{q}}_s$ dofs may then be evaluated through (37) in a post-processing calculation. One may notice that the second line of Eq. (38) could also be condensed statically. However, this must be done after assembling to ensure continuity of the nodal electrical dofs. Hence, the elementary system (38) is assembled to get the corresponding global stiffness matrices, $\mathbf{K}_m^*$, $\mathbf{K}_{me}^*$, $\mathbf{K}_{ee}^*$, and mechanical and electrical load vectors, $\mathbf{F}_m$, $\mathbf{F}_{ma}^*$, $\mathbf{F}_{mc}$, $\mathbf{F}_{ea}^*$ and $\mathbf{F}_{ec}$, leading to

$$\begin{bmatrix} \mathbf{K}_m^* & -\mathbf{K}_{me}^* \\ -\mathbf{K}_{me}^{*\mathrm{t}} & \mathbf{K}_{ee}^* \end{bmatrix} \begin{Bmatrix} \mathbf{q}_m \\ \mathbf{q}_e \end{Bmatrix} = \begin{Bmatrix} \mathbf{F}_m + \mathbf{F}_{ma}^* + \mathbf{F}_{mc} \\ \mathbf{F}_{ea}^* - \mathbf{F}_{ec} \end{Bmatrix} \tag{41}$$

The second line of Eq. (41) allows the static condensation of the assembled vector of nodal electrical dofs, $\mathbf{q}_e$. This is achieved by solving the second line of (41) for $\mathbf{q}_e$, leading to

$$\mathbf{q}_e = \mathbf{K}_{ee}^{*-1}\left(\mathbf{K}_{me}^{*\mathrm{t}}\mathbf{q}_m + \mathbf{F}_{ea}^* - \mathbf{F}_{ec}\right) \tag{42}$$

Then, replacing $\mathbf{q}_e$ in the first line of (41), it is possible to write the equilibrium equations for the nodal mechanical dofs $\mathbf{q}_m$ as

$$\begin{aligned} \left(\mathbf{K}_m^* - \mathbf{K}_{me}^*\mathbf{K}_{ee}^{*-1}\mathbf{K}_{me}^{*\mathrm{t}}\right)\mathbf{q}_m = \mathbf{F}_m + \left(\mathbf{F}_{mc} - \mathbf{K}_{me}^*\mathbf{K}_{ee}^{*-1}\mathbf{F}_{ec}\right) \\ + \left(\mathbf{F}_{ma}^* + \mathbf{K}_{me}^*\mathbf{K}_{ee}^{*\ -1}\mathbf{F}_{ea}^*\right) \end{aligned} \tag{43}$$

The solution of (43) not only leads to faster calculations since matrices dimensions are lower but also prevents ill-conditioning problems of solving directly Eq. (41). Therefore, both piezoelectric actuators and sensors can be considered in a closed-loop analysis. The finite element matrices were obtained through analytic (exact) integration. The choice of a quadratic section rotation β_c is coherent with the cubic transverse deflection w, hence there is no need of a special numerical integration scheme, such as reduced integration.

4. RESULTS AND COMPARISONS

In this section, the results obtained with the proposed FE model are compared with the existing analytical and FE results found in the literature for a sandwich beam with a continuous piezoceramic core. Then, the proposed model is used to evaluate the effects of TSDT and third-order electric potential on the results of a more realistic case of a small piezoceramic patch embedded in an elastic core (discontinuous core). For that, let us consider the shear actuated cantilever beam, presented by Sun and Zhang [1, 2] and shown in Figure 2, consisting of a cantilever sandwich beam with length 100 mm and composed of two aluminum faces, each with 8 mm thickness, and a 2 mm thickness foam core. For the continuous core case, a PZT5H piezoceramic layer covers the entire core (Figure 2a), whereas, for the discontinuous core case, a PZT5H piezoceramic patch with length 10 mm is inserted in the core 10 mm away from the clamped end, replacing the existing foam (Figure 2b). Aluminum properties are: Young's modulus $E_b = 70.3$ GPa and Poisson's ratio $\nu = 0.345$. Those of the foam are: Young's modulus $E_f = 35.3$ MPa and shear modulus $G_f = 12.7$ MPa; and, for the PZT5H: $c_{33}^* = 60.9$ GPa, $c_{55} = 23$ GPa, piezoelectric coupling constants $e_{33}^* = 27.6$ C m^{-2}, $e_{15} = 17$ C m^{-2}, and dielectric constants $\epsilon_{11} = 1.503\,10^{-8}$ F m^{-1} and $\epsilon_{33}^* = 1.334\,10^{-8}$ F m^{-1}.

4.1. Cantilever Sandwich Beam with a Shear Piezoceramic Actuator Core Layer

First, the sandwich beam with a continuous PZT5H piezoceramic core (Figure 2a) is used as an example to compare the results found with the present FE model, using 40 elements, to the analytical results presented by Zhang and Sun [2] and Aldraihem and Khdeir [6], and to the FE results presented by Benjeddou et al. [3, 4]. Notice that the analytical results of Zhang

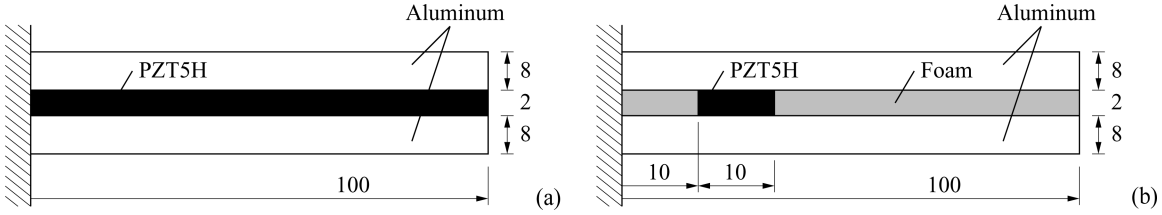

FIG. 2. Cantilever sandwich beam with embedded shear piezoceramic material (dimensions in mm and not in scale). (a) Continuous core case, (b) Discontinuous core case.

and Sun [2] were found using an assumption of a linear electric potential through the piezoceramic core thickness combined to a classical sandwich beam theory (i.e., Euler-Bernoulli faces and Timoshenko core). On the other hand, Aldraihem and Khdeir [6] used an equivalent single layer (ESL) model for the sandwich beam, for which the shear strain is represented by first-order (FSDT, i.e., Timoshenko) and third-order (TSDT, Reddy [19]) theories. Although not stated in their text, it appears that Aldraihem and Khdeir [6] also consider a linear through-thickness electric potential for the piezoceramic core.

In order to bend the beam, a voltage of 20 V is applied between the top and bottom surfaces of the piezoelectric core. Hence, a through-thickness electric field is induced, which in turns induces a shear strain, in the piezoelectric core. Figure 3 shows the resulting deflection of the sandwich beam along its length evaluated using Zhang and Sun's analytical sandwich FSDT solution [2], Aldraihem and Khdeir's analytical ESL TSDT solution [6], Benjeddou et al.'s sandwich FSDT FE model [3, 4] and the present sandwich TSDT FE model. In addition, Figure 3 also presents the results found when the contributions of Ψ_3, corresponding to the third-order term in the electric potential, are neglected. Notice that the latter case corresponds to the assumption of a linear through-thickness electric potential in the core. As already shown in a previous work [3, 4], the FSDT FE model results match very well the analytical ones presented by Zhang and Sun [2]. However, as can be observed in Figure 3 and also in Figure 5a of [6], the ESL TSDT model of Aldraihem and Khdeir [6] is stiffer than the sandwich FSDT model of Zhang and Sun [2]. Indeed, the results obtained with the present TSDT FE model using a linear electric potential also indicate that the inclusion of variable shear strains may lead to a stiffer model

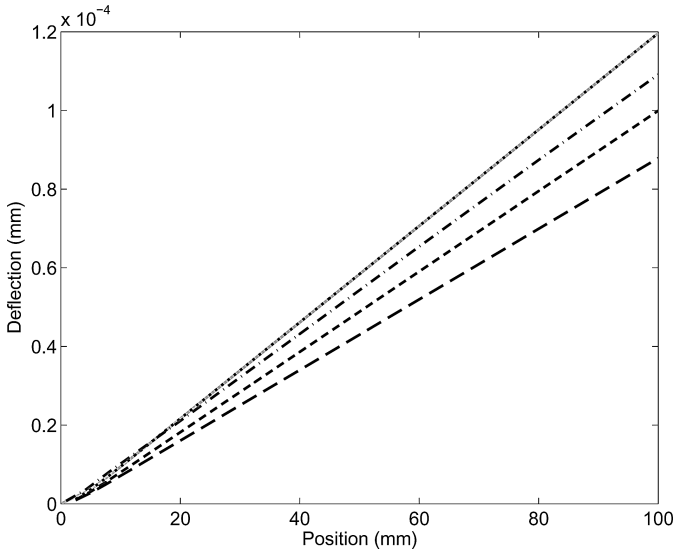

FIG. 3. Sandwich beam deflection along longitudinal direction. —: FSDT analytic [2], · · ·: FSDT FE [3, 4], –·–: ESL TSDT analytic [6], - - -: Present TSDT FE with linear electric potential, – –: Present TSDT FE with cubic electric potential.

TABLE 1
Tip deflection due to a 20 V voltage applied to the shear piezoelectric core

	Tip deflection (μm)
FSDT analytic [2]	0.1196
FSDT FE [3, 4]	0.1196
ESL TSDT analytic [6]	0.1091
Present TSDT FE, linear electric potential	0.0999
Present TSDT FE, cubic electric potential	0.0879

(Figure 3). It is also shown in Figure 3 that the assumption of a cubic electric potential for the piezoelectric core leads to an additional bending stiffness. This may be explained by the fact that, even for an applied (prescribed) difference of electric potential to the upper and lower surfaces of a piezoelectric shear actuator, there exists another contribution to the electric potential induced in the piezoelectric material. Then, this third-order induced electric potential leads to an augmentation of both bending and shear stiffness of the core. This combined electromechanical coupling yields an overall stiffer structure, as shown in Figure 3 for the present TSDT FE with cubic electric potential. For further reference, the tip deflection obtained by the different models is presented in Table 1.

4.2. Cantilever Sandwich Beam with an Embedded Shear Piezoceramic Patch

In this section, the proposed FE model is used to perform a comparative analysis between FSDT and TSDT solutions for the more realistic case of a discontinuous piezoceramic core (Figure 2b). For that, two conditions are studied: 1) an electric potential of 20 V is applied to the piezoceramic patch, and 2) a transverse mechanical force of 10 N applied to the sandwich beam at 3 cm from the clamped end. In both cases, 48 finite elements are used, 10 along the piezoceramic patch and 38 distributed along the rest of the beam. In the first case, a difference of electric potential $V_c^{(0)}$ is prescribed and the resulting deflection, shear strains, and electric field are evaluated using a FSDT FE model, presented in [4, 17], and the present TSDT FE model with cubic electric potential. In the second case, the difference of electric potential $V_c^{(0)}$ is unknown and induced by the beam deformation. In this case, deflection, shear strains, and electric field are also evaluated. Notice, however, that in both cases (electrical or mechanical load), the third-order term of the electric potential in the core is induced and, thus, the electric field must be evaluated after the beam deformation.

4.2.1. Actuation Behavior

Figure 4 shows the sandwich beam deflection along the longitudinal direction induced by a difference of potential of 20 V applied to the piezoceramic core, acting as a piezoelectric shear actuator. Notice that, as for the continuous case, the TSDT model

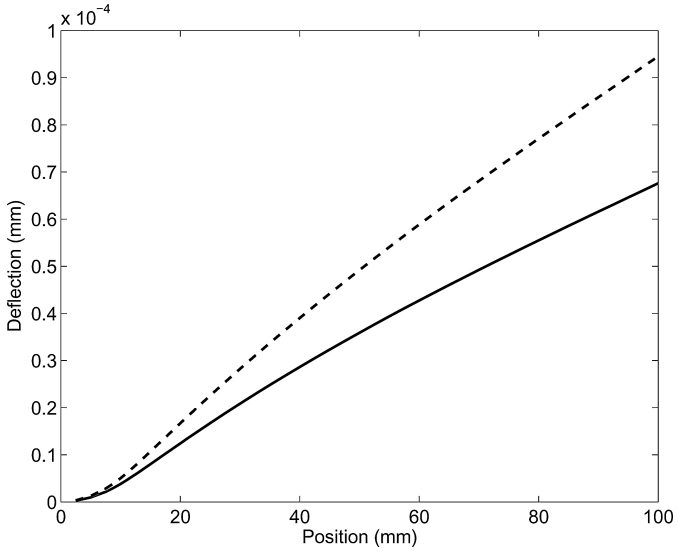

FIG. 4. Sandwich beam deflection along longitudinal direction induced by an applied voltage to the piezoceramic patch. —: TSDT, - - -: FSDT.

yields a stiffer structure than the FSDT model. This extra stiffness appears to be due to both the third-order strain and the induced electric potential in the piezoelectric core.

As explained previously, although an electric difference of potential is applied at the upper and lower surfaces of the piezoelectric actuator and, thus, the electric potentials at the surfaces are completely defined, the resulting deformation of the piezoelectric material leads also to an induced potential. Hence, the electric field shall be variable along the core thickness. As shown in Figure 5, only the TSDT model is able to represent the through-thickness variation of the electric field. Analysis of TSDT model results (Figure 5) also shows that the electric field is stronger at the piezoelectric core surfaces

TABLE 2
Mechanical and electrical quantities induced by a 20 V voltage applied to the shear piezoelectric patch

	Tip deflection (μm)	Maximum shear strain in the core (μm/m)	Electric field Ez (V/mm)
FSDT	0.0945	7.2949	10
TSDT	0.0676	8.0370	6.94–16.11

and smaller near its center. This effect may explain the smaller actuation performance of the shear actuator shown in Figure 4 and Table 2, since the actual electrical field applied to the shear actuator is smaller where the shear strain is expected to be maximum.

The shear strains induced in the core due to the applied voltage are shown in Figures 6 and 7, using FSDT and TSDT models respectively. As expected, both models yield similar shear strain behavior along the longitudinal direction. However, only the TSDT model is able to represent the quadratic variation of shear strains in the thickness direction. Moreover, Table 2 shows that the maximum shear strain in the core for the TSDT model (at $x = 17$ mm and $z = 0$ mm) is higher than that for the FSDT model (at $x = 18$ mm, constant in z). Notice that, for the TSDT model, the shear strains vanish at the piezoelectric core upper and lower surfaces. Hence, this leads also to a continuity of shear strains between the sandwich beam core and faces, since the faces were assumed not to present shear strains (Euler-Bernoulli hypotheses). This effect may also explain the smaller deflection of the sandwich beam (Figure 4) when using the TSDT model, since the equivalent forces actuating the beam faces depend on the shear stress at the interfaces, which vanish for the TSDT model.

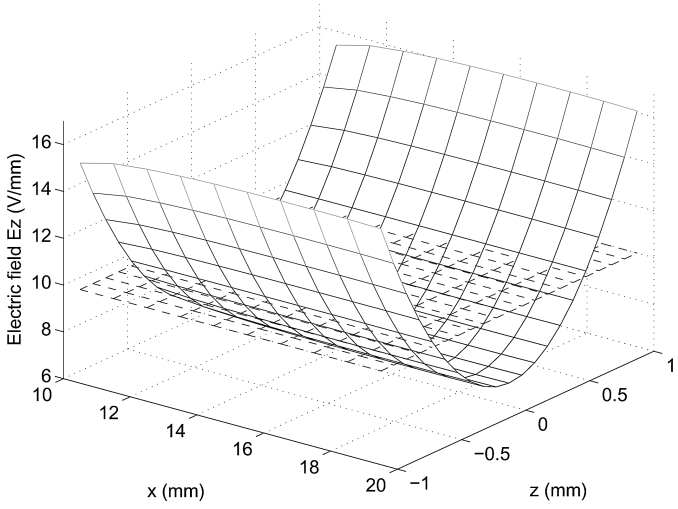

FIG. 5. Electric field E_z in the core along longitudinal and thickness directions, for electrical load, using TSDT (solid line) and FSDT (dashed line).

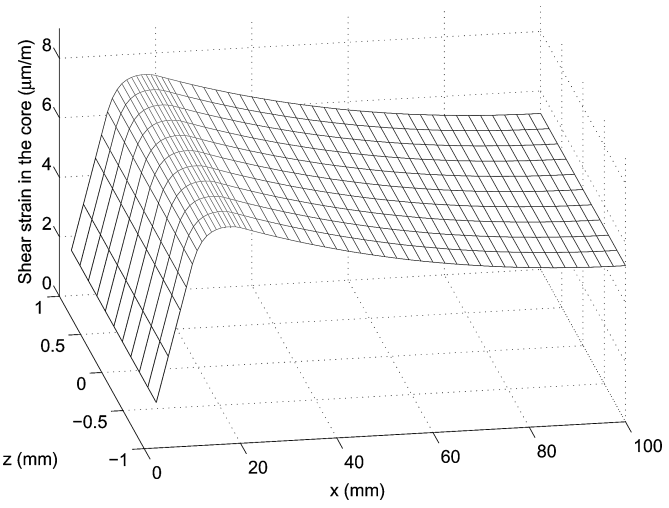

FIG. 6. Shear strain in the core along longitudinal and thickness directions, for electrical load, using FSDT.

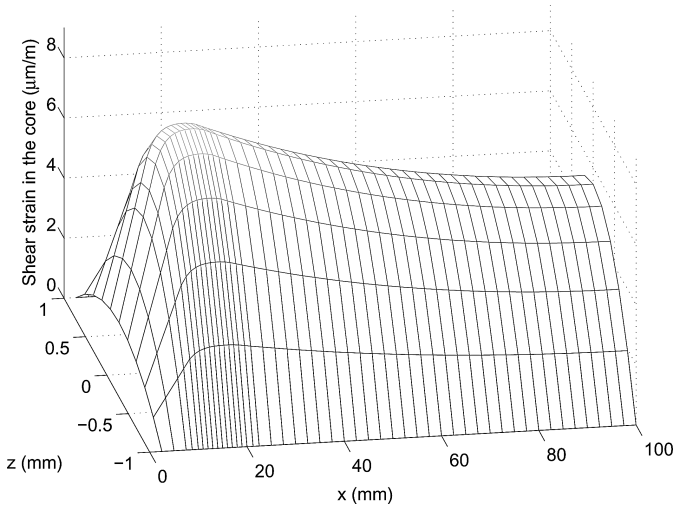

FIG. 7. Shear strain in the core along longitudinal and thickness directions, for electrical load, using TSDT.

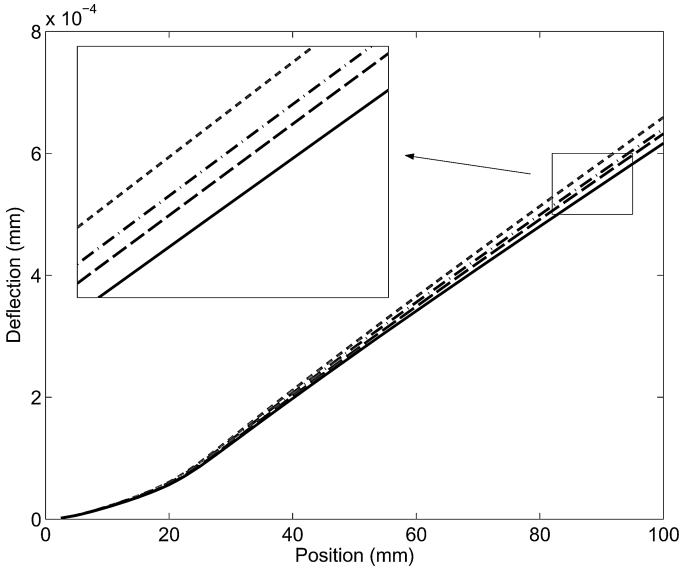

FIG. 8. Sandwich beam deflection along longitudinal direction induced by an applied transversal force. - - -: FSDT without induced potential, —·—: TSDT without induced potential, – –: FSDT, —: TSDT.

4.2.2. *Sensing Behavior*

It is also worthwhile to evaluate the sensor aspect of the piezoelectric material. This is done here through the evaluation of the deformation and electric potential induced in the piezoceramic core when a mechanical transversal force of 10 N is applied to the sandwich beam at 3 cm from the clamped end, using FSDT and TSDT models. This mechanical force is expected to induce large shear strain variations near the piezoceramic patch. Notice that, in this case, both linear and cubic parts of the electric potential, that is V_c and Ψ_3, are induced by the mechanical deformation of the piezoelectric core. However, due to the electromechanical coupling between electrical and mechanical variables, V_c with ε_c^s, and Ψ_3 with ε_c^b, ε_c^h and ε_c^s, the induced electric potential also leads to a stiffening of the piezoelectric core (both in shear and bending). Figure 8 shows the sandwich beam deflection along the longitudinal direction induced by the applied transversal force evaluated using FSDT and TSDT models, with and without induced potential. As for the applied voltage case, here the TSDT model also leads to smaller deflections than FSDT model, due to a stiffening of the structure (see also Table 3). It can also be observed from Figure 8 that the induced potential (V_c for FSDT, and V_c and Ψ_3 for TSDT) does increase the stiffness of the piezoelectric core.

TABLE 3
Deflection and strain induced by a 10 N transversal force applied to the sandwich beam at 3 cm from the clamped end

	Tip deflection (μm)	Maximum shear strain in the core (μm/m)
FSDT without induced potential	0.6592	—
TSDT without induced potential	0.6402	—
FSDT	0.6322	18.4884
TSDT	0.6167	26.4054

It is also worthwhile to analyze the shear strains induced by the applied mechanical load. Figure 9 shows shear strains in the core neutral line along longitudinal direction, evaluated using FSDT and TSDT models. It can be observed that the longitudinal variation of the shear strain is quite similar for FSDT and TSDT. Although not shown in the figure, for the through-thickness behavior the expected constant, for FSDT, and quadratic, for

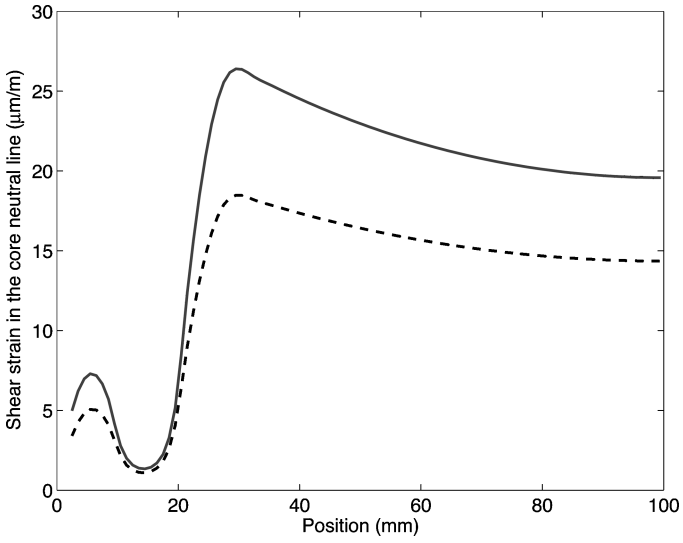

FIG. 9. Shear strain in the core neutral line along longitudinal direction induced by an applied transversal force, using FSDT (dashed line) and TSDT (solid line).

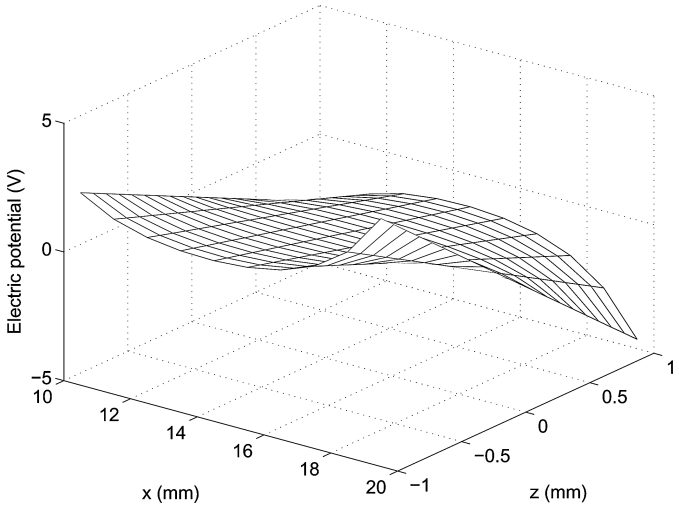

FIG. 10. Electric potential in the core along longitudinal and thickness directions, for mechanical load, using FSDT.

TSDT, shear strains were observed. Notice that although the overall deflection of the sandwich beam is smaller when evaluated using the TSDT model (Figure 8), the shear strains in the elastic/piezoelectric core are larger (Figure 9 and Table 3).

Figures 10 and 11 show the electric potential in the core along longitudinal and thickness directions induced by the sandwich beam deformation, using FSDT and TSDT models. It indicates quite similar results for the electric potential, excepted for the through-thickness nonlinear behavior present only in TSDT model. Although, the third-order term of the electric potential appears to have little effect on the electric potential, it does affect the mechanical response due to the electromechanical coupling between Ψ_3 and bending, shear and third-order core strains, as observed in Figure 8.

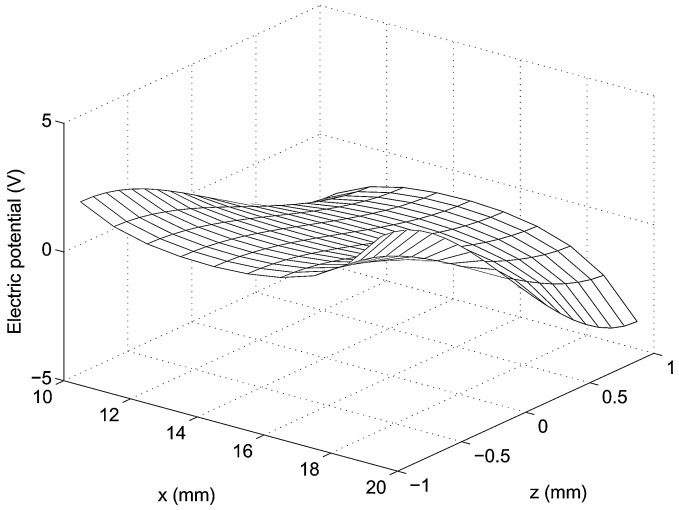

FIG. 11. Electric potential in the core along longitudinal and thickness directions, for mechanical load, using TSDT.

5. CONCLUSIONS AND PERSPECTIVES

A higher-order sandwich beam electromechanical model based on a refinement of CST, where the core is modelled with a TSDT, was proposed. It was shown that the electromechanical coupling with the higher-order strains requires a third-order through-thickness approximation for the electric potential. Using these assumptions, a FE model was developed and, then, compared with analytical and numerical CST and analytical ESL models for a continuous piezoceramic core. It was shown that even when acting as an actuator, there exists a third-order induced potential in the piezoceramic material which may yield an overall stiffer structure. A comparison between FSDT and TSDT FE results for piezoceramic sensor and actuator embedded in an elastic core was also performed to evaluate the electrical and mechanical model refinement. For the actuator case, analysis of TSDT model results has shown that the electric field is stronger at the piezoelectric core surfaces and smaller near its center. It was also observed that the vanishing shear strains at the piezoelectric core upper and lower surfaces, for TSDT model, may also explain the smaller deflection of the sandwich beam, since the equivalent forces actuating the beam faces depend on the shear stress at the interfaces. For the sensor case, it was shown that although the overall deflection of the sandwich beam induced by a mechanical transversal force is smaller when evaluated using the TSDT model, the shear strains in the elastic/piezoelectric core are larger. Also, although the third-order term of the electric potential appears to have little effect on the electric potential, it does affect the mechanical response due to its electromechanical coupling with bending, shear and third-order core strains. Notice that the proposed model is limited to extension and bending vibrations of straight beams with rectangular cross section. Extension to torsional vibrations and more general cross sections can be considered as a future work.

Research on the extension of the present FE model to allow dynamic analyses of sandwich beams with embedded shear piezoceramic sensors and actuators is being conducted. Therefore, it is expected that the comparison with recently published experimental results for the vibration of a cantilever sandwich beam with embedded shear piezoceramic patches [20] will allow a better evaluation of the effectiveness of the present model. The development of a new FE model allowing a non null shear stress at the interfaces is also being conducted.

REFERENCES

1. Sun, C. T., and Zhang, X. D., "Use of thickness-shear mode in adaptive sandwich structures," *Smart Materials and Structures* **4**(3), 202–206 (1995).
2. Zhang, X. D., and Sun, C. T., "Formulation of an adaptive sandwich beam," *Smart Materials and Structures* **5**(6), 814–823 (1996).
3. Benjeddou, A., Trindade, M. A., and Ohayon, R., "A unified beam finite element model for extension and shear piezoelectric actuation mechanisms," *Journal of Intelligent Material Systems and Structures* **8**(12), 1012–1025 (1997).

4. Benjeddou, A., Trindade, M. A., and Ohayon, R., "New shear actuated smart structure beam finite element," *AIAA Journal* **37**(3), 378–383 (1999).
5. Benjeddou, A., Trindade, M. A., and Ohayon, R., "Piezoelectric actuation mechanisms for intelligent sandwich structures," *Smart Materials and Structures* **9**(3), 328–335 (2000).
6. Aldraihem, O. J., and Khdeir, A. A., "Smart beams with extension and thickness-shear piezoelectric actuators," *Smart Materials and Structures* **9**(1), 1–9 (2000).
7. Khdeir, A. A., and Aldraihem, O. J., "Deflection analysis of beams with extension and shear piezoelectric patches using discontinuity functions," *Smart Materials and Structures* **10**(2), 212–220 (2001).
8. Aldraihem, O. J., and Khdeir, A. A., "Exact deflection solutions of beams with shear piezoelectric actuators," *International Journal of Solids and Structures* **40**(1), 1–12 (2003).
9. Trindade, M. A., Benjeddou, A., and Ohayon, R., "Parametric analysis of the vibration control of sandwich beam through shear-based piezoelectric actuation," *Journal of Intelligent Materials Systems and Structures*, **10**(5), 377–385 (1999).
10. Raja, S., Prathap, G., and Sinha, P. K., "Active vibration control of composite sandwich beams with piezoelectric extension-bending and shear actuators," *Smart Materials and Structures* **11**(1), 63–71 (2002).
11. Raja, S., Sreedeep, R., and Prathap, G., "Bending behavior of hybrid-actuated piezoelectric sandwich beams," *Journal of Intelligent Materials Systems and Structures* **15**(8), 611–619 (2004).
12. Vel, S. S., and Batra, R. C., "Exact solution for the cylindrical bending of laminated plates with embedded piezoelectric shear actuators," *Smart Materials and Structures* **10**(2), 240–251 (2001).
13. Edery-Azulay, L., and Abramovich, H., "Piezoelectric actuation and sensing mechanisms—closed form solutions," *Composite Structures* **64**(3–4), 443–453 (2004).
14. Benjeddou, A., "Modelling and simulation of adaptive structures and composites: Current trends and future directions," in B. H. V. Topping and C.A. Mota Soares (Eds.), *Progress in Computational Structures Technology*, Saxe-Coburg Pub., Stirling, Scotland, pp. 251–280 (2004).
15. Benjeddou, A., "Use of shear-mode piezoceramics in smart structures applications: Achievements and perspectives," in C. A. Mota Soares et al. (Eds.), *II ECCOMAS Thematic Conference on Smart Structures and Materials*, Lisbon, Portugal, July 18–21 (2005).
16. Mota Soares, C. A., Mota Soares, C. M., and Franco Correia, V. M., "Modelling and design of laminated composite structures with integrated sensors and actuators," in B. H. V. Topping (Ed.), *Computational Mechanics for the Twenty-First Century*, Saxe-Coburg Pub., Edinburg, UK, vol. 9, pp. 165–185 (2000).
17. Trindade, M. A., Benjeddou, A., and Ohayon, R., "Finite element modeling of hybrid active-passive vibration damping of multilayer piezoelectric sandwich beams—part 1: Formulation," *International Journal for Numerical Methods in Engineering* **51**(7), 835–854 (2001).
18. Abramovich, H., "Piezoelectric actuation for smart sandwich structures—closed form solutions," *Journal of Sandwich Structures and Materials* **5**(4), 377–396 (2003).
19. Reddy, J. N., "A simple higher-order theory for laminated composite plates," *Journal of Applied Mechanics* **51**(4), 745–752 (1984).
20. Baillargeon, B. P., and Vel, S. S., "Active vibration suppression of sandwich beams using piezoelectric shear actuators: Experiments and numerical simulations," *Journal of Intelligent Materials Systems and Structures*, **16**(6), 517–530 (2005).